# Unlocking the Potential of Linear Networks for Irregular Multivariate Time Series Forecasting

Chengsen Wang, Qi Qi, Jingyu Wang, Haifeng Sun, Zirui Zhuang, Jianxin Liao

Beijing University of Posts and Telecommunications, Beijing, China {cswang, qiqi8266, wangjingyu, hfsun, zhuangzirui, liaojx}@bupt.edu.cn

#### Abstract

Time series forecasting holds significant importance across various industries, including finance, transportation, energy, healthcare, and climate. Despite the widespread use of linear networks due to their low computational cost and effectiveness in modeling temporal dependencies, most existing research has concentrated on regularly sampled and fully observed multivariate time series. However, in practice, we frequently encounter irregular multivariate time series characterized by variable sampling intervals and missing values. The inherent intra-series inconsistency and inter-series asynchrony in such data hinder effective modeling and forecasting with traditional linear networks relying on static weights. To tackle these challenges, this paper introduces a novel model named AiT. AiT utilizes an adaptive linear network capable of dynamically adjusting weights according to observation time points to address intra-series inconsistency, thereby enhancing the accuracy of temporal dependencies modeling. Furthermore, by incorporating the Transformer module on variable semantics embeddings, AiT efficiently captures variable correlations, avoiding the challenge of inter-series asynchrony. Comprehensive experiments across four benchmark datasets demonstrate the superiority of AiT, improving prediction accuracy by 11% and decreasing runtime by 52% compared to existing state-of-the-art methods.

## 1 Introduction

Time series forecasting has played a pivotal role across various industries, including finance [1], transportation [9], energy [21], healthcare [15], and climate [44]. With the development of deep learning techniques, neural network-based methods have notably propelled advancements owing to their strong capability in capturing various dependencies. The relevant models have evolved from statistical models [3] to RNNs [10], CNNs [29], GNNs [30], and Transformers [17]. Recently, linear networks [36] have garnered considerable attention because of low computational overhead and effectiveness in modeling temporal dependencies. The iTransformer [19] enhances linear networks by incorporating the attention mechanism to capture variable correlations, representing a State-Of-The-Art (SOTA) approach that optimally balances efficiency and accuracy.

Although time series forecasting has been widely studied, most research [18] has concentrated on Regular Multivariate Time Series (RMTS) with consistent sampling intervals and complete observations. Conversely, less attention has been given to Irregular Multivariate Time Series (IMTS), which feature variable sampling intervals and missing data. In practice, obtaining regular and complete observations for all variables is challenging due to the high sampling costs and the intrinsic difficulties in entirely averting equipment failures. For instance, long-term monitoring of patients

<sup>\*</sup>Equal contribution.

<sup>†</sup>Corresponding author.

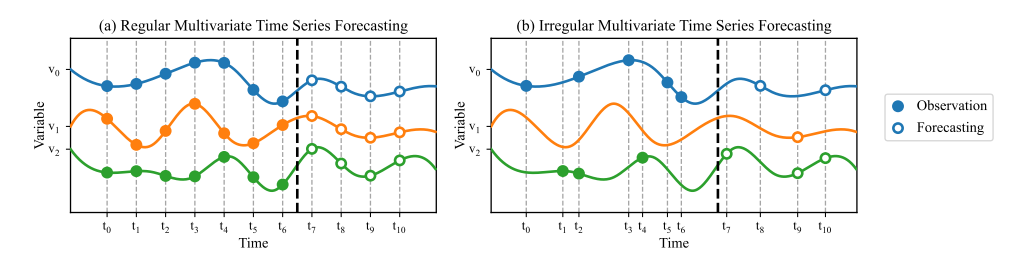


Figure 1: The comparison of regular multivariate time series forecasting and irregular multivariate time series forecasting.

with chronic illnesses frequently generates multiple irregular time series of physiological metrics. This irregularity arises because it is impractical for patients to undergo uniform examinations at strictly fixed intervals, compounded by occasional malfunctions in home monitoring devices. While some recent studies [24] have made strides in IMTS forecasting, they typically emphasize modeling temporal dependencies within series using neural Ordinary Differential Equations (ODEs) [8] without explicitly addressing the variable correlations. Moreover, the numerical integration in ODE solvers is computationally intensive [2], leading to low efficiency in training and inference.

As illustrated in Figure 1, the modeling of IMTS is more complex than RMTS due to the inherent intra-series inconsistency and inter-series asynchrony. (1) Intra-series inconsistency. In RMTS, observations are recorded at fixed intervals, ensuring that each period contains a uniform number of observations, with each observation corresponding to a specific time point. Given this consistency, traditional linear networks [36] can effectively capture temporal dependencies through weighted summation based on a static weight matrix. In contrast, in IMTS, variable sampling intervals and missing values lead to a fluctuating number of observations within the same period across different samples and variables, with identical observation locations potentially corresponding to different time points. This inconsistency of time points, both in length and value, may cause shape mismatches and numerical misalignments for a static weight matrix. (2) Inter-series asynchrony. Although strong correlations often exist between different variable series, irregular sampling or missing data can lead to misalignment in IMTS observations. Such asynchrony may obscure or distort the relationships between variables, hindering the accurate identification of their correlations.

To address these challenges, we propose a novel IMTS forecasting model. Given historical observations and forecasting queries, IMTS forecasting aims to forecast future values corresponding to these queries accurately. We begin by independently embedding the raw series of each variable in IMTS using a Temporal Encoder, which generates a representation vector to capture temporal dependencies. To achieve this, we introduce an Adaptive Linear (ALinear) network that dynamically adjusts weights based on observed time points, enabling the Temporal Encoder to handle intra-series inconsistencies in historical data effectively. Subsequently, a Spatial Encoder, composed of stacked Transformer [27] blocks, is applied to these variable embeddings to capture variable correlations. Modeling correlations at the latent representation space efficiently mitigates the challenge of inter-series asynchrony. Finally, the comprehensive latent representations for each variable are independently mapped to the forecasting series via the Predictor, which also employs ALinear to manage intra-series inconsistencies in the forecasting queries. In contrast to iTransformer [19], the SOTA method in RMTS, our approach just replaces the standard linear networks in both the Temporal Encoder and Predictor with ALinear. Accordingly, this new method is named AiT (Adaptive iTransformer).

The contributions of our paper are summarised as follows:

- We present ALinear, which adaptively adjusts weights based on observation time points and effectively addresses intra-series inconsistency in IMTS. Experimental results demonstrate that it successfully bridges the gap between regular and irregular time series.
- We introduce a novel IMTS forecasting method AiT, which addresses inherent challenges of inconsistency and asynchrony while exhibiting superiority in modeling temporal dependencies and variable correlations.
- We evaluate AiT through extensive experiments on four publicly available IMTS datasets.
   The findings indicate that AiT provides significant advantages in both prediction accuracy and computational efficiency.

## 2 Related Work

## 2.1 Regular Multivariate Time Series Forecasting

As a significant real-world challenge, time series forecasting has garnered considerable attention. Initially, ARIMA [3] establishes an autoregressive model and performs forecasts in a moving average manner. However, the inherent complexity of the real world often renders it challenging to adapt. With the development of deep learning techniques, neural network-based methods have become increasingly important. RNNs [10] dynamically capture temporal dependencies by modeling semantic information within a sequential structure. Unfortunately, this architecture suffers from gradient vanishing/exploding and information forgetting when dealing with long sequences. To further improve prediction performance, CNNs [29] and self-attention mechanisms [20, 42] have been introduced to capture long-range dependencies. Moreover, GNNs [6, 14, 31, 32, 34] have also been further integrated into multivariate time series analysis due to their outstanding capability to model complex variable correlations.

Linear networks [36] have recently demonstrated remarkable capacity in capturing temporal dependencies. In contrast to more complex models, linear networks exhibit lower computational overhead while achieving comparable and occasionally superior prediction accuracy. Building upon the use of linear networks for capturing temporal dependencies, iTransformer [19] supplements the Transformer architecture to model variable correlations. By embedding series from distinct variables into individual tokens for the subsequent attention mechanism, iTransformer strikes an optimal balance between efficiency and accuracy, establishing itself as the SOTA approach for RMTS forecasting.

#### 2.2 Irregular Multivariate Time Series Analysis

Existing research in IMTS primarily concentrates on classification [7, 12, 37, 41] and imputation [25] tasks, with limited attention to forecasting. GRU-D [7], a model based on gated recurrent units, employs time decay and missing data imputation strategies to address irregularly sampled time series. mTAND [25] is an IMTS imputation model that can be easily applied to forecasting tasks by only replacing the queries for imputation with forecasting. It learns embeddings for numerical values corresponding to continuous time steps and generates fixed-length representations for variable-length sequential data using an attention mechanism.

Recently, several prospective studies have focused on forecasting tasks in IMTS. Specifically, these studies [2, 5, 22, 23] mainly utilize neural ODEs and concentrate on addressing continuous dynamics and inconsistency. However, the computation of ODE solvers is widely acknowledged as inefficient due to the substantial cost associated with numerical integration. Furthermore, although these studies have made significant progress in addressing inconsistencies within irregular time series, the effective modeling of variable correlations within asynchronous IMTS [33] remains an underexplored domain. Recently, T-PatchGNN [39] proposed a transformable patch method for converting univariate irregular time series into temporally aligned patches. These patches are then fed into the Transformer module and the temporal adaptive GNN to capture temporal dependencies and dynamic variable correlations. The time-aligned patches position T-PatchGNN as a SOTA approach for IMTS forecasting tasks, optimizing both efficiency and accuracy.

## 3 Methodology

#### 3.1 Problem Definition

An IMTS with N variables can be represented as  $\mathcal{O} = \left\{\mathbf{o}_{1:L_n}^n\right\}_{n=1}^N = \left\{[(t_i^n, x_i^n)]_{i=1}^{L_n}\right\}_{n=1}^N$ , where the n-th variable contains  $L_n$  observations. The i-th observation of the n-th variable is composed of the recorded time point  $t_i^n$  and the corresponding value  $x_i^n$ . The time point  $t_i^n$  are arranged chronologically, with the intervals between neighboring time points being variable. Due to the irregular sampling intervals and the occurrence of missing values, different samples or variables may exhibit varying numbers of observations  $L_n$  within the same time span. Furthermore, even the same observation position i may correspond to different actual time point  $t_i^n$ .

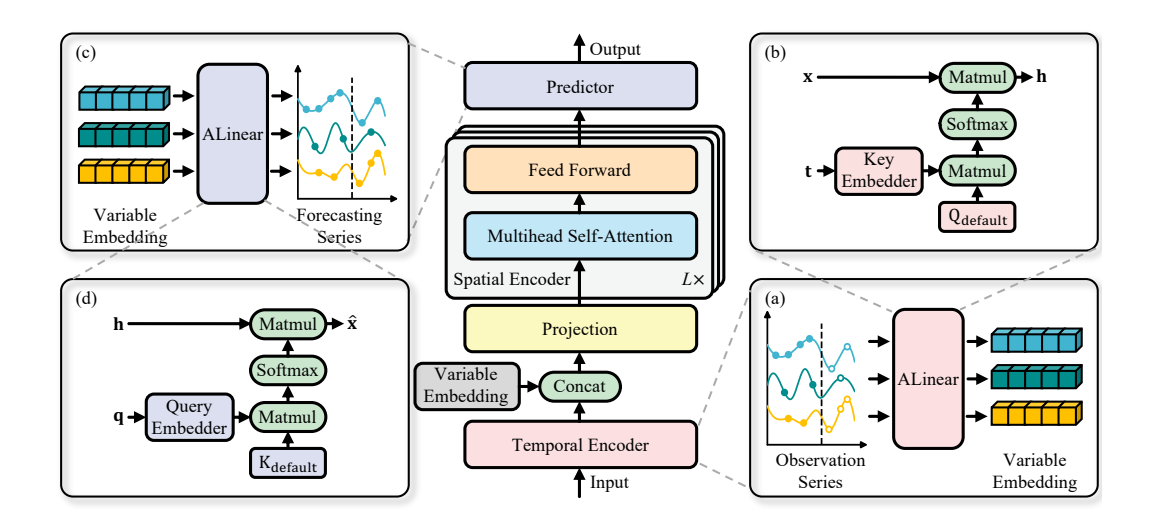


Figure 2: The overall framework of AiT. Raw observation series from different variables are independently embedded into dynamic variable embeddings via the Temporal Encoder. The Projection then integrates dynamic and static variable embeddings. The aggregated variable embedding is subsequently fed into the Spatial Encoder to capture variable correlations. Finally, the Predictor individually transforms the embedding of each variable into the forecasting series.

Given historical IMTS observations  $\mathcal{O} = \left\{ \left[ (t_i^n, x_i^n) \right]_{i=1}^{L_n} \right\}_{n=1}^N$  and a set of forecasting queries  $\mathcal{Q} = \left\{ \left[ q_j^n \right]_{j=1}^{Q_n} \right\}_{n=1}^N$ , where the n-th variable includes  $Q_n$  queries, each query  $q_j^n$  represents the j-th request to predict the value of the n-th variable at a future time step. The objective of IMTS forecasting is to predict the target values  $\hat{\mathcal{X}} = \left\{ \left[ \hat{x}_j^n \right]_{j=1}^{Q_n} \right\}_{n=1}^N$  corresponding to these queries. This forecasting task can be formulated as:

$$\mathcal{F}(\mathcal{O}, \mathcal{Q}) \longrightarrow \hat{\mathcal{X}}$$
 (1)

where  $\mathcal{F}(\cdot)$  denotes the forecasting model to be learned.

#### 3.2 Framework Overview

The overall architecture of AiT is illustrated in Figure 2 and comprises three essential components: a Temporal Encoder, a Spatial Encoder, and a Predictor. Initially, the Temporal Encoder models the temporal dependencies of irregularly sampled observation series  $\mathbf{x}^n \in \mathbb{R}^{L_n}$  for each variable, embedding them independently into fixed-length dynamic variable representation  $\mathbf{h}^n_{\text{dyna}} \in \mathbb{R}^D$ , where D denotes the dimension of the hidden embedding. Acknowledging that some variables may lack observations entirely, we introduce a learnable static variable representation  $\mathbf{h}^n_{\text{dyna}}$  to supplement the information. Subsequently, this concatenated variable representation is projected back to the original dimension  $\mathbf{h}^n \in \mathbb{R}^D$  through a MultiLayer Perceptron (MLP). Next, the Spatial Encoder employs stacked Transformer blocks to capture variable correlations further. The challenge of inter-series asynchrony is adeptly circumvented by implementing the Multi-head Self-Attention (MSA) mechanism [27] within the latent representation space. Ultimately, the Predictor receives the comprehensive latent embeddings of each variable and independently transforms them into the forecasting series  $\hat{\mathbf{x}}^n \in \mathbb{R}^{Q_n}$ . To address the challenges posed by intra-series inconsistency in historical observations and forecasting queries, we implement the Temporal Encoder and Predictor using the meticulously designed ALinear.

## 3.3 Adaptive Linear

In RMTS, the fixed and equal observation intervals allow traditional linear networks [36] to effectively capture temporal dependencies through weighted summation based on a static weight matrix.

However, in IMTS with variable sampling intervals and missing values, the number of observations and their corresponding time points within the same period vary, resulting in shape mismatches and numerical misalignments for the static weight matrix. To address this issue, we propose an adaptive linear network to bridge the gap between regular and irregular time series. With an integrated attention mechanism [27], ALinear dynamically adjusts the weight assignments based on actual time points in historical observations and forecasting queries, ensuring consistent representations for observation series obtained from different locations within the same series.

Given the input data  $\mathbf{x} \in \mathbb{R}^{L_{in}}$  and its associated time point  $\mathbf{s} \in \mathbb{R}^{L_{in}}$ , the objective of ALinear is to produce the value  $\mathbf{y} \in \mathbb{R}^{L_{out}}$  corresponding to the output time point  $\mathbf{t} \in \mathbb{R}^{L_{out}}$ . In IMTS, the input length  $L_{in}$  and the output length  $L_{out}$  typically vary across samples or variables. ALinear first extracts high dimensional features from the input time point  $\mathbf{s}$  and output time point  $\mathbf{t}$  using the Key Embedder and Query Embedder, respectively, converting them into keys  $\mathbf{K} \in \mathbb{R}^{L_{in} \times D}$  and queries  $\mathbf{Q} \in \mathbb{R}^{L_{out} \times D}$ :

$$\mathbf{K} = \text{KeyEmbedder}(\mathbf{s})$$

$$\mathbf{Q} = \text{QueryEmbedder}(\mathbf{t})$$
(2)

To maintain architectural simplicity, both the Key Embedder and Query Embedder are constructed using an MLP comprising two layers of linear transformations and an activation function of ReLU [11]. Subsequently, ALinear derives the dynamic weight matrix  $\mathbf{W} \in \mathbb{R}^{L_{out} \times L_{in}}$  by calculating the dot product attention between  $\mathbf{Q}$  and  $\mathbf{K}$ . To ensure the consistency of output expectation across varying input lengths  $L_{in}$ , we implement the function Softmax [4] to normalize the weights. The final weight  $\mathbf{W}$  which can adaptively adjust its shape and value in accordance with time points, is employed to weight the input  $\mathbf{x}$  for summation. The entire process can be expressed as:

$$\mathbf{W} = \mathbf{Q}\mathbf{K}^{\mathrm{T}}$$

$$\mathbf{W} = \operatorname{Softmax}(\mathbf{W})$$

$$\mathbf{v} = \mathbf{W}\mathbf{x}$$
(3)

Additionally, when the input time point  $\mathbf{s}$  (output time point  $\mathbf{t}$ ) is absent or remains constant, ALinear will utilize the built-in learnable matrix  $\mathbf{K}_{\text{default}} \in \mathbb{R}^{L_{in} \times D}$  ( $\mathbf{Q}_{\text{default}} \in \mathbb{R}^{L_{out} \times D}$ ) to substitute for the output of the Key Embedder (Query Embedder), thereby ensuring compatibility with the functionality of the standard linear networks. The comprehensive flow of ALinear is summarized in Algorithm 1. A detailed comparative analysis of Adaptive Linear and standard Linear is provided in Appendix A.

#### 3.4 Temporal Encoder

In this section, we employ a consistent processing procedure for all univariate time series and describe it in detail using the n-th variable as a case study. As illustrated in Figure 2(a), the Temporal Encoder is tasked with modeling the temporal dependencies within the n-th variable observation series  $\mathbf{x}^n$  and converting it into a fixed-length dynamic variable representation  $\mathbf{h}_{\text{dyna}}^n$ . Given the challenges posed by variable sampling intervals and missing values in IMTS, we select ALinear to implement the Temporal Encoder. Specifically, as depicted in Figure 2(b), since the output length D remains constant, ALinear utilizes the built-in learnable matrix  $\mathbf{Q}_{\text{default}}$  and Key Embedder to facilitate this process, mathematically represented as:

$$\mathbf{h}_{\text{dyna}}^{n} = \text{ALinear} (\mathbf{x} = \mathbf{x}^{n}, \mathbf{s} = \mathbf{t}^{n}, \mathbf{t} = \emptyset)$$
 (4)

Furthermore, in instances where no observations are available, we introduce an additional learnable static variable representation for the n-th variable, denoted as  $\mathbf{h}_{\text{stat}}^n$ , which is integrated with the dynamic features  $\mathbf{h}_{\text{dyna}}^n$  generated from ALinear previously to mitigate the potential information loss. Subsequently, this concatenated variable representation is processed through an MLP comprising two layers of linear transformations and an activation function of ReLU, which ultimately maps back to the original dimension  $\mathbf{h}^n$ . The following equation can summarize this process:

$$\mathbf{h}^{n} = \text{MLP}\left(\mathbf{h}_{\text{dyna}}^{n} || \mathbf{h}_{\text{stat}}^{n}\right)$$
 (5)

where the notation || represents the concatenation operation between vectors.

Through the aforementioned temporal embedding and feature fusion processes, raw observation series of varying lengths can be transformed into feature representations of uniform dimension. Consequently, each IMTS instance can be comprehensively represented by a shape-fixed embedding matrix  $\mathbf{H} \in \mathbb{R}^{N \times D} = \{\mathbf{h}^n\}_{n=1}^N$ .

#### 3.5 Spatial Encoder

Although significant correlations typically exist between the series of different variables, observations within IMTS may be considerably misaligned due to irregular sampling or missing values [39]. This asynchrony can obscure or distort the actual relationships among variables, posing a substantial challenge in accurately capturing variable correlations. The Spatial Encoder adeptly circumvented inter-series asynchrony by employing the MSA [27] within the latent representation space and capturing variable correlations at different levels using Transformer blocks stacked with L layers. The entire process can be succinctly expressed by the following equation:

$$\mathbf{H}^{l+1} = \text{TransformerBlock}(\mathbf{H}^l), \ l = 0, \cdots, L-1$$
 (6)

where  $\mathbf{H}^l \in \mathbb{R}^{N \times D}$  represents the intermediate representation vector output from the l-th layer of Transformer block.

Each Transformer block comprises two principal components: a multi-head self-attention mechanism and a feed-forward network. The self-attention mechanism generates query, key, and value vectors by applying a linear transformation to the representation embeddings of each variable. The attention scores computed from the dot product between the query and the key signify the variable correlations [19]. Consequently, variables that exhibit strong correlations will be assigned more weighted for the subsequent representation interaction with values. The feed-forward networks employ dense nonlinear connections to extract deeper features from time series. Recent revisiting on linear predictors [36] highlights that temporal features extracted by MLPs are supposed to be shared within distinct time series. The neurons of MLP are trained to portray the intrinsic properties of any time series.

#### 3.6 Predictor

In this section, we employ a consistent processing procedure for all univariate time series and describe it in detail using the n-th variable as a case study. The generation of forecasting series is performed by the linear network within the Predictor, whose superiority has been validated by numerous prior studies [19]. As illustrated in Figure 2(c), the Predictor independently projects the comprehensive latent embedding  $\mathbf{h}^n$  of the n-th variable back into the data space to generate the forecasting series  $\hat{\mathbf{x}}^n$ . To tackle the challenge of intra-series inconsistency, we adopt ALinear, which adaptively adjusts the weight assignment based on actual time points, as the core component of the Predictor. Specifically, as depicted in Figure 2(d), since input length D remains constant, ALinear utilizes the built-in learnable matrix  $\mathbf{K}_{\text{default}}$  and Query Embedder to facilitate this process, mathematically represented as:

$$\hat{\mathbf{x}}^n = \text{ALinear}(\mathbf{x} = \mathbf{h}^n, \mathbf{s} = \emptyset, \mathbf{t} = \mathbf{q}^n)$$
 (7)

Finally, the AiT is trained by minimizing the Mean Squared Error (MSE) between the prediction and the ground truth:

$$\mathcal{L} = \frac{1}{N} \sum_{n=1}^{N} \frac{1}{Q_n} \sum_{j=1}^{Q_n} (\hat{x}_j^n - x_j^n)^2$$
 (8)

## 4 Experiment

#### 4.1 Experimental Setup

#### 4.1.1 Dataset

To evaluate the prediction performance, we adhere to established mainstream protocols [39] and perform extensive experiments on four real-world datasets (PhysioNet, MIMIC, Activity, and USHCN). Please refer to Appendix B.1 for details of these datasets.

#### 4.1.2 Baseline

To establish a comprehensive benchmark for the IMTS forecasting task, we integrate 20 relevant baselines for a fair comparison, encompassing RMTS forecasting (iTransformer [19], DLinear [36], TimesNet [29], PatchTST [20], Crossformer [42], GraphWavenet [31], MTGNN [32], StemGNN [6], CrossGNN [14], and FourierGNN [34]), IMTS classification (GRU-D [7], SeFT [12], RainDrop [41],

Table 1: The prediction errors of AiT and baselines for irregular multivariate time series forecasting. The results of iTransformer and GraFITi are reproduced from their official implementations and other results are taken from T-PatchGNN. A lower value denotes superior prediction accuracy. The optimal and suboptimal results are highlighted in bold and underlined, respectively.

36.1.1	PhysioNet	MIMIC	Activity	USHCN	
Method	$\frac{1}{\text{MSE}\times10^{-3}}\frac{\text{MAE}\times10^{-2}}{\text{MSE}\times10^{-2}}$	MSE×10 <sup>-2</sup> MAE×10 <sup>-2</sup>	MSE×10 <sup>-3</sup> MAE×10 <sup>-2</sup>	$\frac{1}{\text{MSE} \times 10^{-1} \text{ MAE} \times 10^{-1}}$	
	MSEX10 MAEX10	MSE×10 MAE×10	MSEXIO MAEXIO	MSEXIO MAEXIO	
iTransformer	$  53.6 \pm 0.63   16.9 \pm 0.51$	$7.28 \pm 0.52  21.4 \pm 0.99$	$3.99 \pm 0.12  4.34 \pm 0.10$	$  6.20 \pm 0.11 \ 4.22 \pm 0.56  $	
DLinear	$41.9 \pm 0.05$ $15.5 \pm 0.03$	$4.90 \pm 0.00  16.3 \pm 0.05$	$4.03 \pm 0.01$ $4.21 \pm 0.01$	$6.21 \pm 0.00$ $3.88 \pm 0.02$	
TimesNet	$16.5 \pm 0.11$ $6.14 \pm 0.03$	$5.88 \pm 0.08  13.6 \pm 0.07$	$3.12 \pm 0.01$ $3.56 \pm 0.02$	$5.58 \pm 0.05$ $3.60 \pm 0.04$	
PatchTST	$12.0 \pm 0.23$ $6.02 \pm 0.14$	$3.78 \pm 0.03$ $12.4 \pm 0.10$	$4.29 \pm 0.14  4.80 \pm 0.09$	$5.75 \pm 0.01$ $3.57 \pm 0.02$	
Crossformer	$6.66 \pm 0.11$ $4.81 \pm 0.11$	$2.65 \pm 0.10$ $9.56 \pm 0.29$	$4.29 \pm 0.20$ $4.89 \pm 0.17$	$5.25 \pm 0.04$ $3.27 \pm 0.09$	
Graph Wavenet	$6.04 \pm 0.28  4.41 \pm 0.11$	$2.93 \pm 0.09  10.5 \pm 0.15$	$2.89 \pm 0.03$ $3.40 \pm 0.05$	$5.29 \pm 0.04$ $3.16 \pm 0.09$	
MTGNN	$6.26 \pm 0.18$ $4.46 \pm 0.07$	$2.71 \pm 0.23$ $9.55 \pm 0.65$	$3.03 \pm 0.03$ $3.53 \pm 0.03$	$5.39 \pm 0.05$ $3.34 \pm 0.02$	
StemGNN	$6.86 \pm 0.28  4.76 \pm 0.19$	$1.73 \pm 0.02$ $7.71 \pm 0.11$	$8.81 \pm 0.37  6.90 \pm 0.02$	$5.75 \pm 0.09$ $3.40 \pm 0.09$	
CrossGNN	$7.22 \pm 0.36  4.96 \pm 0.12$	$2.95 \pm 0.16  10.8 \pm 0.21$	$3.03 \pm 0.10$ $3.48 \pm 0.08$	$5.66 \pm 0.04$ $3.53 \pm 0.05$	
FourierGNN	$6.84 \pm 0.35  4.65 \pm 0.12$	$2.55 \pm 0.03$ $10.2 \pm 0.08$	$2.99 \pm 0.02$ $3.42 \pm 0.02$	$5.82 \pm 0.06$ $3.62 \pm 0.07$	
GRU-D	$  5.59 \pm 0.09   4.08 \pm 0.05$	$1.76 \pm 0.03$ $7.53 \pm 0.09$	$2.94 \pm 0.05$ $3.53 \pm 0.06$	$5.54 \pm 0.38$ $3.40 \pm 0.28$	
SeFT	$9.22 \pm 0.18$ $5.40 \pm 0.08$	$1.87 \pm 0.01  7.84 \pm 0.08$	$12.2 \pm 0.17$ $8.43 \pm 0.07$	$5.80 \pm 0.19$ $3.70 \pm 0.11$	
RainDrop	$9.82 \pm 0.08  5.57 \pm 0.06$	$1.99 \pm 0.03$ $8.27 \pm 0.07$	$14.9 \pm 0.14  9.45 \pm 0.05$	$5.78 \pm 0.22$ $3.67 \pm 0.17$	
Warpformer	$5.94 \pm 0.35  4.21 \pm 0.12$	$1.73 \pm 0.04  7.58 \pm 0.13$	$2.79 \pm 0.04$ $3.39 \pm 0.03$	$5.25 \pm 0.05$ $3.23 \pm 0.05$	
mTAND	$6.23 \pm 0.24  4.51 \pm 0.17$	$1.85 \pm 0.06  7.73 \pm 0.13$	$3.22 \pm 0.07$ $3.81 \pm 0.07$	$5.33 \pm 0.05$ $3.26 \pm 0.10$	
Latent-ODE	$6.05 \pm 0.57  4.23 \pm 0.26$	$1.89 \pm 0.19$ $8.11 \pm 0.52$	$3.34 \pm 0.11$ $3.94 \pm 0.12$	$5.62 \pm 0.03$ $3.60 \pm 0.12$	
CRU	$8.56 \pm 0.26$ $5.16 \pm 0.09$	$1.97 \pm 0.02  7.93 \pm 0.19$	$6.97 \pm 0.78  6.30 \pm 0.47$	$6.09 \pm 0.17$ $3.54 \pm 0.18$	
Neural Flow	$7.20 \pm 0.07  4.67 \pm 0.04$	$1.87 \pm 0.05$ $8.03 \pm 0.19$	$4.05 \pm 0.13$ $4.46 \pm 0.09$	$5.35 \pm 0.05$ $3.25 \pm 0.05$	
GraFITi	$5.36 \pm 0.28  4.04 \pm 0.19$	$1.78 \pm 0.06$ $7.36 \pm 0.26$	$3.24 \pm 0.51$ $3.58 \pm 0.37$	$5.09 \pm 0.05$ $3.10 \pm 0.05$	
T-PatchGNN	$4.98 \pm 0.08$ $3.72 \pm 0.03$	$1.69 \pm 0.03$ $7.22 \pm 0.09$	$2.66 \pm 0.03$ $3.15 \pm 0.02$	$5.00 \pm 0.04$ $3.08 \pm 0.04$	
Ours	$4.58 \pm 0.06$ $3.39 \pm 0.02$	$1.27 \pm 0.02$ $6.16 \pm 0.08$	$2.37 \pm 0.02$ $2.93 \pm 0.02$	$ \hline   \   \textbf{4.43} \pm \textbf{0.03} \   \textbf{3.03} \pm \textbf{0.03} \\ \hline$	
Impr.	8.45 %	19.77 %	8.94 %	6.64 %	

and Warpformer [37]), IMTS imputation (mTAND [25]), and IMTS forecasting (Latent-ODE [22], CRU [23], Neural Flow [2], GraFITi [33], and T-PatchGNN [39]). The details of these baselines are provided in Appendix B.2.

#### **4.1.3** Metric

Most existing IMTS forecasting studies rely primarily on MSE for evaluation, which is highly sensitive to outliers. To ensure a more robust assessment of model performance, we also adopt the MAE, a metric widely used in RMTS evaluations [19]. The formal definitions of these metrics are as [39]: MSE =  $\frac{1}{N} \sum_{n=1}^{N} \frac{1}{Q_n} \sum_{j=1}^{Q_n} \left( \hat{x}_j^n - x_j^n \right)^2$ , MAE =  $\frac{1}{N} \sum_{n=1}^{N} \frac{1}{Q_n} \sum_{j=1}^{Q_n} \left| \hat{x}_j^n - x_j^n \right|$ . Lower values of MSE and MAE indicate higher prediction accuracy.

The details of experimental setup can be found in Appendix B.3. All experiments are repeated five times with different random seeds, and the statistical result is reported.

## 4.2 Main Result

Table 1 presents the MSE and MAE evaluation results of AiT against 20 relevant baselines across four datasets. These findings demonstrate that AiT consistently achieves superior performance.

Modeling and forecasting IMTS is more challenging than RMTS due to inherent intra-series inconsistency and inter-series asynchrony. Experimental results demonstrate that algorithms designed explicitly for RMTS are significantly less effective when applied to IMTS. iTransformer and DLinear, which utilize static weights to model temporal dependencies, consistently performs the worst across nearly all datasets. This underscores the necessity of developing ALinear. Moreover, while previous work [43] has often affirmed the superiority of disregarding variable correlations in RMTS forecasting, this conclusion does not appear to hold for IMTS. Our study indicates that algorithms incorporating variable correlations (e.g., Crossformer and FourierGNN) generally outperform models that rely solely on single-variable information (e.g., TimesNet and PatchTST) in IMTS contexts. This difference may arise because, in RMTS, the excess information leads models to overfit and misgeneralize variable correlations from the training set to the test set [35]. In contrast, in the IMTS setting, sparse observations alone are insufficient to provide a solid foundation for future predictions, making incorporating information from other relevant variables a valuable complementary approach.

Table 2: The average training time per epoch and total inference time of AiT and baselines for irregular multivariate time series forecasting. A lower value denotes greater efficiency. The optimal and suboptimal results are highlighted in bold and underlined, respectively.

	PhysioNet		MIMIC		Activity		USHCN	
Method	Training Time (s)	Inference Time (s)						
GRU-D	76.62	10.06	511.8	24.99	39.52	0.769	131.9	8.762
SeFT	106.7	7.406	378.6	25.85	22.70	1.510	84.15	9.770
RainDrop	86.71	6.641	286.3	27.41	19.56	1.396	51.99	8.706
Warpformer	12.88	8.997	80.93	27.68	5.117	1.323	19.65	5.826
mTAND	9.754	2.623	31.13	5.829	1.964	0.415	6.926	2.830
Latent-ODE	2796.	55.99	6915.	128.7	454.8	3.695	1971.	38.82
CRU	855.0	95.86	2642.	263.0	194.4	13.94	734.9	102.9
Neural Flow	715.2	21.16	1895.	77.99	139.7	5.897	347.2	25.23
GraFITi	435.6	12.24	1193.	39.11	110.2	1.944	231.3	19.14
T-PatchGNN	7.312	1.622	25.42	4.318	1.721	0.233	5.281	1.477
Ours	2.291	0.372	12.78	1.841	1.022	0.114	4.212	0.691
Impr.	72.90 %		53.55 %		46.44 %		36.66 %	

Among baselines for IMTS analysis, those focused on imputation and forecasting outperform algorithms centered on classification. This disparity arises primarily because different tasks necessitate distinct representations: the former demands fine-grained representations, while the latter emphasizes coarse-grained modeling [29]. Furthermore, baselines based on RNNs for capturing temporal dependencies (e.g., CRU and Latent-ODE) are less effective than T-PatchGNN, which leverages attention mechanisms for modeling temporal dependencies. This is due to the inherent limitations of RNNs, including vanishing/exploding gradients and information loss in long sequences [18]. However, previous studies [19, 36] have shown that this temporal dependencies modeling approach, based on the patch+attention architecture, is inferior to linear networks in both prediction accuracy and computational efficiency. AiT effectively addresses the challenge of intra-series inconsistency in IMTS scenarios by introducing an adaptive linear network. Extensive empirical analysis confirms its superiority on modeling temporal dependencies and variable correlations.

To further investigate the impact of ALinear on model efficiency, we compare the average training time per epoch and overall inference time. Table 2 shows that AiT substantially outperforms all IMTS analysis methods. Owing to the lower computational demands of linear networks, AiT reduces training time by 44.81% and inference time by 59.68% compared to the SOTA method T-PatchGNN, which utilizes the patch+transformer architecture. In addition, we also explore the forecasting performance of AiT under various historical and forecasting horizons, as well as the applicability of ALinear in RMTS forecasting. The results are summarized in Appendix C.2 and Appendix C.3.

## 4.3 Ablation Study

In order to validate the effectiveness and reasonableness of each component, we evaluate the performance of AiT and its variants on all datasets. (1) **rp TTCN**: We substitute ALinear in the Temporal Encoder with a Transformable Time-aware Convolution Network (TTCN) [40]. (2) **rp TempTF**: We substitute ALinear in the Temporal Encoder with the Transformer+Pool architecture. (3) **rm SpatTF**: We remove the Spatial Encoder. (4) **rm StatVE**: We remove the static variable representation  $\mathbf{h}_{\text{stat}}^n$ . (5) **rp TsMLP**: We replace ALinear in the Predictor with an MLP architecture. The Appendix B.4 provides a detailed description of these variants.

The findings of the ablation study are presented in Table 3, where "rp" denotes the replacement operation and "rm" signifies the removal operation. Additionally, we evaluate the average training time per epoch and the overall inference time on two datasets, MIMIC, which encompasses the greatest number of variables, and USHCN, which contains the highest number of samples. The experimental results are summarized in Figure 3. The outcomes indicate that either replacing or removing any component results in a decline in prediction accuracy relative to the complete model.

To assess the advantages of ALinear in modeling temporal dependencies, we replace the ALinear in the Temporal Encoder with the TTCN and TempTF, commonly utilized in previous IMTS forecasting frontier algorithms [38, 39]. The results indicate that the performance of TTCN is comparable to that of ALinear. However, TTCN employs a masking mechanism within a high-dimensional hidden space

Table 3: The prediction errors of AiT and its variants for irregular multivariate time series forecasting. A lower value denotes superior prediction accuracy. The optimal results are highlighted in bold.

Method	PhysioNet		MIMIC		Activity		USHCN		Impr.
	$MSE \times 10^{-3}$	$MAE \times 10^{-2}$	$MSE \times 10^{-2}$	${ m MAE}{ imes}10^{-2}$	$MSE \times 10^{-3}$	${ m MAE}{ imes}10^{-2}$	MSE×10 <sup>-1</sup>	$MAE \times 10^{-1}$	
Ours	$\textbf{4.58} \pm \textbf{0.06}$	$\textbf{3.39} \pm \textbf{0.02}$	$\textbf{1.27} \pm \textbf{0.02}$	$\textbf{6.16} \pm \textbf{0.08}$	$\textbf{2.37} \pm \textbf{0.02}$	$\textbf{2.93} \pm \textbf{0.02}$	$  4.43 \pm 0.03$	$\textbf{3.03} \pm \textbf{0.03}$	0.00%
rp TTCN	$4.60 \pm 0.13$	$3.43 \pm 0.04$	$1.32 \pm 0.04$	$6.29 \pm 0.10$	$2.41 \pm 0.03$	$2.96 \pm 0.02$	$  5.61 \pm 0.06$	$3.60 \pm 0.04$	-7.37%
rp TempTF	$4.64 \pm 0.09$	$3.42 \pm 0.07$	$1.32 \pm 0.04$	$6.37 \pm 0.08$	$2.46 \pm 0.07$	$3.02 \pm 0.02$	$8.74 \pm 0.45$	$5.75 \pm 0.18$	-26.9%
rm SpatTF	$4.88 \pm 0.06$	$3.51 \pm 0.03$	$1.38 \pm 0.02$	$6.29 \pm 0.10$	$2.77 \pm 0.04$	$3.14 \pm 0.02$	$5.27 \pm 0.04$	$3.29 \pm 0.07$	-8.47%
rm StatVE	$7.14 \pm 0.09$	$4.17 \pm 0.06$	$2.75 \pm 0.02$	$9.58 \pm 0.11$	$2.63 \pm 0.01$	$3.11 \pm 0.03$	$5.25 \pm 0.03$	$3.24 \pm 0.02$	-34.5%
rp TsMLP	$4.63\pm0.09$	$3.43\pm0.06$	$1.29\pm0.04$	$6.27\pm0.12$	$2.47\pm0.03$	$3.02 \pm 0.04$	$4.56 \pm 0.06$	$3.12\pm0.03$	-2.29%

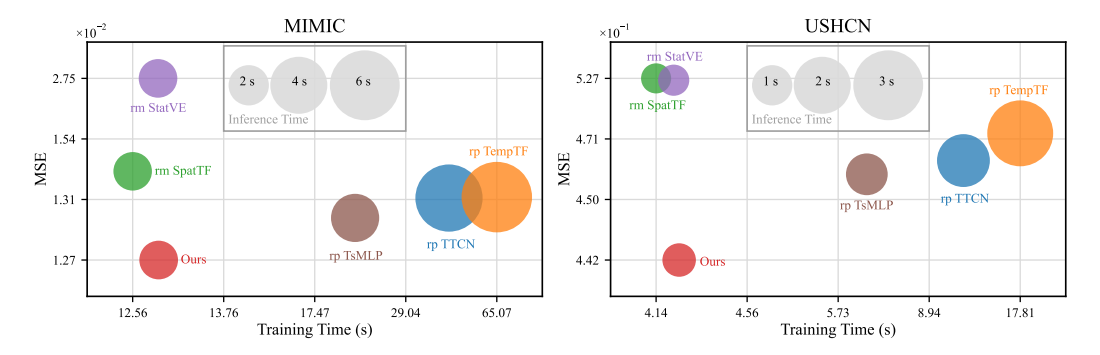


Figure 3: The prediction error, average training time per epoch, and total inference time of AiT and its variants for irregular multivariate time series forecasting. A lower value denotes a better performance.

to address the challenge of missing values in IMTS. This operation, which is more computationally intensive, led to an increase of 195.28% in training time and a 175.40% rise in inference time. TempTF achieves competitive prediction accuracy across most datasets, with the exception of USHCN, which features short horizon lengths and a limited number of variables. The sparse observations and diminished correlations among variables hinder the complex Transformer architecture from extracting sufficient information efficiently. Additionally, the square computational complexity resulting from the self-attention mechanism between time points substantially escalates the computational burden, increasing 366.09% and 259.55% in training and inference times, respectively.

Sparse observations in IMTS are typically insufficient for accurate predictions, making integrating information from other relevant variables an effective complementary approach. Removing the Spatial Encoder results in a performance decline of 8.47%. Additionally, we observe that the Spatial Encoder does not impose a significant computational cost, as the attention mechanism operates across a limited number of variables [19]. The static variable representation mitigates the issue of insufficient information caused by high missing rates or even complete absence. Once this representation is removed, substantial performance degradation is observed across all datasets, with a particularly pronounced impact on datasets with high missing rates, such as PhysioNet and MIMIC. Finally, using TsMLP as an alternative led to the most minor performance reduction. However, MLP operations based on high-dimensional hidden vector concatenation introduce more computational overhead compared to ALinear, increasing training and inference times by 58.54% and 55.27%, respectively.

## 5 Conclusion

In this study, we extend the highly anticipated linear networks from RMTS to IMTS. We have meticulously designed an adaptive linear network, ALinear, which dynamically adjusts weights based on observation time points and effectively addresses intra-series inconsistency in IMTS. Experimental results demonstrate that ALinear successfully bridges the gap between regular and irregular time series, showcasing its superiority in modeling and forecasting both series. Building on this innovation, we propose a novel IMTS forecasting model, AiT, by substituting the conventional linear networks in the Temporal Encoder and Predictor of iTransformer with ALinear. Experimental results across four benchmark datasets indicate that AiT significantly outperforms existing methods in terms of both prediction accuracy and computational efficiency.

#### References

- [1] Adebiyi Ariyo Ariyo, Aderemi Oluyinka Adewumi, and Charles K. Ayo. Stock price prediction using the ARIMA model. In *International Conference on Computer Modelling and Simulation*, 2014.
- [2] Marin Bilos, Johanna Sommer, Syama Sundar Rangapuram, Tim Januschowski, and Stephan Günnemann. Neural flows: Efficient alternative to neural odes. In *Annual Conference on Neural Information Processing Systems*, 2021.
- [3] G. E. P. Box and G. M. Jenkins. Some recent advances in forecasting and control. *Journal of the Royal Statistical Society*, 17, 1968.
- [4] John S. Bridle. Training stochastic model recognition algorithms as networks can lead to maximum mutual information estimation of parameters. In *Annual Conference on Neural Information Processing Systems*, 1989.
- [5] Edward De Brouwer, Jaak Simm, Adam Arany, and Yves Moreau. Gru-ode-bayes: Continuous modeling of sporadically-observed time series. In *Annual Conference on Neural Information Processing Systems*, 2019.
- [6] Defu Cao, Yujing Wang, Juanyong Duan, Ce Zhang, Xia Zhu, Congrui Huang, Yunhai Tong, Bixiong Xu, Jing Bai, Jie Tong, and Qi Zhang. Spectral temporal graph neural network for multivariate time-series forecasting. In *Annual Conference on Neural Information Processing Systems*, 2020.
- [7] Zhengping Che, Sanjay Purushotham, Kyunghyun Cho, David A. Sontag, and Yan Liu. Recurrent neural networks for multivariate time series with missing values. *arXiv*, 1606.01865, 2016.
- [8] Tian Qi Chen, Yulia Rubanova, Jesse Bettencourt, and David Duvenaud. Neural ordinary differential equations. In *Annual Conference on Neural Information Processing Systems*, 2018.
- [9] Yuzhou Chen, Ignacio Segovia-Dominguez, Baris Coskunuzer, and Yulia R. Gel. Tamps2gcnets: Coupling time-aware multipersistence knowledge representation with spatio-supra graph convolutional networks for time-series forecasting. In *International Conference on Learning Representations*, 2022.
- [10] Valentin Flunkert, David Salinas, and Jan Gasthaus. Deepar: Probabilistic forecasting with autoregressive recurrent networks. *arXiv*, 2201.00382, 2017.
- [11] Xavier Glorot, Antoine Bordes, and Yoshua Bengio. Deep sparse rectifier neural networks. In International Conference on Artificial Intelligence and Statistics, 2011.
- [12] Max Horn, Michael Moor, Christian Bock, Bastian Rieck, and Karsten M. Borgwardt. Set functions for time series. In *International Conference on Machine Learning*, 2020.
- [13] Edward J. Hu, elong Shen, Phillip Wallis, Zeyuan Allen-Zhu, Yuanzhi Li, Shean Wang, Lu Wang, and Weizhu Chen. Lora: Low-rank adaptation of large language models. In *International Conference on Learning Representations*, 2022.
- [14] Qihe Huang, Lei Shen, Ruixin Zhang, Shouhong Ding, Binwu Wang, Zhengyang Zhou, and Yang Wang. Crossgnn: Confronting noisy multivariate time series via cross interaction refinement. In Annual Conference on Neural Information Processing Systems, 2023.
- [15] Shruti Kaushik, Abhinav Choudhury, Pankaj Kumar Sheron, Nataraj Dasgupta, Sayee Natarajan, Larry A. Pickett, and Varun Dutt. AI in healthcare: Time-series forecasting using statistical, neural, and ensemble architectures. *Frontiers Big Data*, 3, 2020.
- [16] Diederik P. Kingma and Jimmy Ba. Adam: A method for stochastic optimization. In *International Conference on Learning Representations*, 2015.
- [17] Yan Li, Xinjiang Lu, Haoyi Xiong, Jian Tang, Jiantao Su, Bo Jin, and Dejing Dou. Towards long-term time-series forecasting: Feature, pattern, and distribution. In *IEEE International Conference on Data Engineering*, 2023.

- [18] Bryan Lim and Stefan Zohren. Time series forecasting with deep learning: A survey. arXiv, 2004.13408, 2020.
- [19] Yong Liu, Tengge Hu, Haoran Zhang, Haixu Wu, Shiyu Wang, Lintao Ma, and Mingsheng Long. itransformer: Inverted transformers are effective for time series forecasting. In *International Conference on Learning Representations*, 2024.
- [20] Yuqi Nie, Nam H. Nguyen, Phanwadee Sinthong, and Jayant Kalagnanam. A time series is worth 64 words: Long-term forecasting with transformers. In *International Conference on Learning Representations*, 2023.
- [21] Tiago Pinto, Isabel Praça, Zita A. Vale, and José Silva. Ensemble learning for electricity consumption forecasting in office buildings. *Neurocomputing*, 423, 2021.
- [22] Yulia Rubanova, Tian Qi Chen, and David Duvenaud. Latent ordinary differential equations for irregularly-sampled time series. In *Annual Conference on Neural Information Processing Systems*, 2019.
- [23] Mona Schirmer, Mazin Eltayeb, Stefan Lessmann, and Maja Rudolph. Modeling irregular time series with continuous recurrent units. In *International Conference on Machine Learning*, 2022.
- [24] Satya Narayan Shukla and Benjamin M. Marlin. A survey on principles, models and methods for learning from irregularly sampled time series: From discretization to attention and invariance. *arXiv*, 2012.00168, 2020.
- [25] Satya Narayan Shukla and Benjamin M. Marlin. Multi-time attention networks for irregularly sampled time series. In *International Conference on Learning Representations*, 2021.
- [26] William Toner and Luke Nicholas Darlow. An analysis of linear time series forecasting models. In *International Conference on Machine Learning*, 2024.
- [27] Ashish Vaswani, Noam Shazeer, Niki Parmar, Jakob Uszkoreit, Llion Jones, Aidan N. Gomez, Lukasz Kaiser, and Illia Polosukhin. Attention is all you need. In *Annual Conference on Neural Information Processing Systems*, 2017.
- [28] Chengsen Wang, Qi Qi, Jingyu Wang, Haifeng Sun, Zirui Zhuang, Jinming Wu, and Jianxin Liao. Rethinking the power of timestamps for robust time series forecasting: A global-local fusion perspective. In *Annual Conference on Neural Information Processing Systems*, 2024.
- [29] Haixu Wu, Tengge Hu, Yong Liu, Hang Zhou, Jianmin Wang, and Mingsheng Long. Timesnet: Temporal 2d-variation modeling for general time series analysis. In *International Conference on Learning Representations*, 2023.
- [30] Jinming Wu, Qi Qi, Jingyu Wang, Haifeng Sun, Zhikang Wu, Zirui Zhuang, and Jianxin Liao. Not only pairwise relationships: Fine-grained relational modeling for multivariate time series forecasting. In *International Joint Conference on Artificial Intelligence*, 2023.
- [31] Zonghan Wu, Shirui Pan, Guodong Long, Jing Jiang, and Chengqi Zhang. Graph wavenet for deep spatial-temporal graph modeling. In *International Joint Conference on Artificial Intelligence*, 2019.
- [32] Zonghan Wu, Shirui Pan, Guodong Long, Jing Jiang, Xiaojun Chang, and Chengqi Zhang. Connecting the dots: Multivariate time series forecasting with graph neural networks. In ACM SIGKDD International Conference on Knowledge Discovery and Data Mining, 2020.
- [33] Vijaya Krishna Yalavarthi, Kiran Madhusudhanan, Randolf Scholz, Nourhan Ahmed, Johannes Burchert, Shayan Jawed, Stefan Born, and Lars Schmidt-Thieme. Grafiti: Graphs for forecasting irregularly sampled time series. In *AAAI Conference on Artificial Intelligence*, 2024.
- [34] Kun Yi, Qi Zhang, Wei Fan, Hui He, Liang Hu, Pengyang Wang, Ning An, Longbing Cao, and Zhendong Niu. Fouriergnn: Rethinking multivariate time series forecasting from a pure graph perspective. In *Annual Conference on Neural Information Processing Systems*, 2023.
- [35] Peiwen Yuan and Changsheng Zhu. Is channel independent strategy optimal for time series forecasting? *arXiv*, 2310.17658, 2023.

- [36] Ailing Zeng, Muxi Chen, Lei Zhang, and Qiang Xu. Are transformers effective for time series forecasting? In *AAAI Conference on Artificial Intelligence*, 2023.
- [37] Jiawen Zhang, Shun Zheng, Wei Cao, Jiang Bian, and Jia Li. Warpformer: A multi-scale modeling approach for irregular clinical time series. In ACM SIGKDD International Conference on Knowledge Discovery and Data Mining, 2023.
- [38] Weijia Zhang, Chenlong Yin, Hao Liu, and Hui Xiong. Unleash the power of pre-trained language models for irregularly sampled time series. *arXiv*, 2408.08328, 2024.
- [39] Weijia Zhang, Chenlong Yin, Hao Liu, Xiaofang Zhou, and Hui Xiong. Irregular multivariate time series forecasting: A transformable patching graph neural networks approach. In *International Conference on Machine Learning*, 2024.
- [40] Weijia Zhang, Le Zhang, Jindong Han, Hao Liu, Yanjie Fu, Jingbo Zhou, Yu Mei, and Hui Xiong. Irregular traffic time series forecasting based on asynchronous spatio-temporal graph convolutional networks. In ACM SIGKDD International Conference on Knowledge Discovery and Data Mining, 2024.
- [41] Xiang Zhang, Marko Zeman, Theodoros Tsiligkaridis, and Marinka Zitnik. Graph-guided network for irregularly sampled multivariate time series. In *International Conference on Learning Representations*, 2022.
- [42] Yunhao Zhang and Junchi Yan. Crossformer: Transformer utilizing cross-dimension dependency for multivariate time series forecasting. In *International Conference on Learning Representations*, 2023.
- [43] Lifan Zhao and Yanyan Shen. Rethinking channel dependence for multivariate time series forecasting: Learning from leading indicators. In *International Conference on Learning Representations*, 2024.
- [44] Yu Zheng, Xiuwen Yi, Ming Li, Ruiyuan Li, Zhangqing Shan, Eric Chang, and Tianrui Li. Forecasting fine-grained air quality based on big data. In *ACM SIGKDD International Conference on Knowledge Discovery and Data Mining*, 2015.

## **A Detailed Analysis of ALinear**

#### Algorithm 1 ALinear

```
1: Parameter: hidden dimension D, input length L_{in} (optional), output length L_{out} (optional)
 2: Input: input data x, input time point s (optional), output time point t (optional)
 3: Output: output data y
 4:
 5: Initialization:
 6: if input length L_{in} is provided then
         Initialize \mathbf{K}_{\text{default}} \in \mathbb{R}^{L_{\text{in}} \times D}
 7:
                                                                                                                  # fixed input time point
 8: end if
 9: if output length L_{\text{out}} is provided then
         Initialize \mathbf{Q}_{\text{default}} \in \mathbb{R}^{L_{\text{out}} \times D}
                                                                                                                # fixed output time point
11: end if
12:
13: Forward Pass:
14: if input time point s is provided then
15:
         \mathbf{K} \leftarrow \text{KeyEmbedder}(\mathbf{s})
                                                                                                             # variable input time point
16: else
17:
         \mathbf{K} \leftarrow \mathbf{K}_{default}
                                                                                                                  # fixed input time point
18: end if
19: if output time point t is provided then
         \mathbf{Q} \leftarrow \text{QueryEmbedder}(\mathbf{t})
                                                                                                            # variable output time point
21: else
22:
         \mathbf{Q} \leftarrow \mathbf{Q}_{\text{default}}
                                                                                                                # fixed output time point
23: end if
24:
25: \mathbf{W} \leftarrow \text{Matmul}(\mathbf{Q}, \mathbf{K}^{T})
26: \mathbf{W} \leftarrow \operatorname{Softmax}(\mathbf{W})
27: \mathbf{y} \leftarrow \operatorname{Matmul}(\mathbf{W}, \mathbf{x})
29: Return y
```

The attention mechanism in ALinear can be considered as a specialized form of a fully connected linear network [36]. While the attention mechanism [27] weights and sums the Value through the product of Query and Key, a traditional fully connected linear network directly applies a weight matrix for weighting and summation. The distinction is that the weights remain static once trained in fully connected linear network, whereas Query and Key are dynamically generated based on input.

In the case of a standard Linear that weights and sums the inputs  $\mathbf{x}$  using fixed weights  $\mathbf{W}_{\text{static}} \in \mathbb{R}^{L_{out} \times L_{in}}$ , the standard Linear and ALinear can be expressed as follows:

$$\mathbf{y}^{L_{out} \times 1} = \left(\mathbf{W}_{\text{static}}^{L_{out} \times L_{in}}\right) \times \mathbf{x}^{L_{in} \times 1}$$

$$\approx \left(\mathbf{Q}_{\text{default}}^{L_{out} \times D} \mathbf{K}_{\text{default}}^{D \times L_{in}}\right) \times \mathbf{x}^{L_{in} \times 1}$$

$$\approx \left(\mathbf{t}^{L_{out} \times 1} \mathbf{E}_{\mathbf{O}}^{1 \times D} \mathbf{E}_{\mathbf{K}}^{D \times 1} \mathbf{s}^{1 \times L_{in}}\right) \times \mathbf{x}^{L_{in} \times 1}$$
(9)

where the Query Embedder and Key Embedder in ALinear are represented by two transformation matrices  $\mathbf{E}_Q \in \mathbb{R}^{1 \times D}$  and  $\mathbf{E}_K \in \mathbb{R}^{1 \times D}$ , respectively, serving the same function. Additionally, the transpose operation of the matrices is omitted to maintain conciseness in the formulas.

For the RMTS forecasting task, the lengths and values of the input and output time points are fixed, allowing the standard linear networks to perform a weighted sum over the input  $\mathbf x$  using the static weight matrix  $\mathbf W_{\text{static}}$ . In this context, ALinear approximates  $\mathbf W_{\text{static}}$  by employing the product of two fixed-shape learnable static low-rank matrices,  $\mathbf Q_{\text{default}}$  and  $\mathbf K_{\text{default}}$ . The experiments detailed in Appendix C.3 indicate that the performance of both approaches is nearly identical. However, when addressing IMTS, the static weight matrix becomes inapplicable due to the variability in the number and actual value of input and output time points. In such cases, ALinear generates dynamic weight matrices that can adaptively modify their shapes and values to approximate  $\mathbf K_{\text{default}}$  ( $\mathbf Q_{\text{default}}$ )

Table 4: The statistics of each dataset.

Dataset	Sample	Variable	Hist	Pred	Sparsity
PhysioNet	12000	41	24 h	24 h	85.74 %
MIMIC	23457	96	24 h	24 h	96.72 %
Activity	5400	12	3000 ms	1000 ms	75.00 %
USHCN	26736	5	24 M	1 M	77.98 %

through the product of the input time point s (output time point t) and the Key Embedder  $\mathbf{E}_K$  (Query Embedder  $\mathbf{E}_Q$ ). This methodology is tantamount to approximating a high-rank matrix with the product of two low-rank matrices of rank 1, which may compromise the fitting capability of the model. Consequently, ALinear favors the utilization of the built-in learnable matrix  $\mathbf{K}_{default}$  ( $\mathbf{Q}_{default}$ ) instead of depending on a learnable time point vector when the input time point s (output time point t) is absent or remains constant. Furthermore, the input time point s, Key Embedder  $\mathbf{E}_K$ , and the learnable matrix  $\mathbf{Q}_{default}$  (as well as the output time point t, Query Embedder  $\mathbf{E}_Q$ , and the learnable matrix  $\mathbf{K}_{default}$ ) can be mixed according to the specific scenario.

## **B** Detailed Experimental Setup

#### **B.1** Dataset

To evaluate the prediction performance, we perform extensive experiments on four real-world datasets. These datasets are widely used for benchmarking and are publicly accessible. Table 4 presents a summary of their statistical characteristics. Samples from each dataset are randomly partitioned into training, validation, and test sets, with a 6:2:2 split ratio. For preprocessing schemes and forecasting configurations, we follow the established mainstream protocols [39]:

- **PhysioNet** <sup>3</sup> contains 12,000 IMTS corresponding to different patients, where each IMTS consists of 41 clinical signal variables irregularly collected within the first 48 hours after patient admission. For each IMTS, we use the first 24 hours as observation data to predict query values for the next 24 hours.
- MIMIC <sup>4</sup> is a widely accessed clinical database. We curated 23,457 IMTS irregularly collected during the first 48 hours after patient admission, with each IMTS containing 96 variables. We utilize the initial 24 hours as observation data to predict target values in the subsequent 24-hour time frame.
- Activity <sup>5</sup> includes 12 variables recorded as irregular measurements of 3D positions from four different sensors placed on the left ankle, right ankle, waist, and chest. To better align with real-world prediction scenarios, we segmented the original time series into chunks, obtaining a total of 5,400 IMTS. Each IMTS spans 4,000 milliseconds, where we use the first 3,000 milliseconds as observation to predict sensor positions in the next 1,000 milliseconds.
- USHCN <sup>6</sup> consists of daily measurements of five climate variables collected between 1996 and 2000 from 1,114 meteorological stations across the United States. To meet practical forecasting requirements, we group the data into 26,736 IMTS. Each IMTS uses the climate data from the preceding 24 months to predict weather for the following month.

#### **B.2** Baseline

To establish a comprehensive benchmark for the IMTS forecasting task, we integrate 20 relevant baselines for a thorough comparison. According to the established mainstream protocols [39], We adapt models associated with RMTS forecasting, IMTS classification, and IMTS imputation to the IMTS forecasting task. To ensure an equitable comparison, we primarily rely on the results presented in T-PatchGNN [39], supplementing them with additional outcomes derived from official implementations within a consistent experimental framework. We search the key hyperparameters of

<sup>3</sup>https://archive.physionet.org/challenge/2012/

<sup>4</sup>https://physionet.org/content/mimiciii/1.4/

<sup>&</sup>lt;sup>5</sup>https://archive.ics.uci.edu/dataset/196/localization+data+for+person+activity

<sup>&</sup>lt;sup>6</sup>https://www.osti.gov/biblio/1394920

these reproduced baselines by exploring values around their recommended configurations and report the optimal results:

- iTransformer [19] embeds individual variable into token employed by the attention mechanism, facilitating the capture of inter-variable multivariate correlations while applying a feed-forward network to each token to acquire nonlinear representations. We use the open source implementation at https://github.com/thuml/Time-Series-Library.
- **DLinear** [36] decomposes time series into trend series and remainder series, subsequently employing two single-layer linear networks to model each of these sequences to accomplish the forecasting task. We use the open source implementation at https://github.com/thuml/Time-Series-Library.
- TimesNet [29] transforms the original series into two-dimensional space based on periodicity, employing CNN to achieve unified modeling of inter-period and intra-period representations. We use the open source implementation at https://github.com/thuml/Time-Series-Library.
- **PatchTST** [20]leverages the Transformer architecture to capture temporal dependencies for forecasting, emphasizing patch and channel independence. We use the open source implementation at https://github.com/thuml/Time-Series-Library.
- **Crossformer** [42] utilizes Cross-Temporal Attention and Cross-Variable Attention to capture temporal dependencies and variable correlations. We use the open source implementation at https://github.com/thuml/Time-Series-Library.
- **GraphWavenet** [31] employs an adaptive adjacency matrix and diffusion convolution to model variable correlations while capturing temporal dependencies through gated mechanisms and dilated causal convolution. We use the official implementation at https://github.com/nnzhan/Graph-WaveNet.
- MTGNN [32] integrates graph convolution networks and temporal convolution networks to capture variable correlations and temporal dependencies. We use the official implementation at https://github.com/nnzhan/MTGNN.
- **StemGNN** [6] transforms the series into the frequency domain using the Fourier transform, thereby capturing temporal-spatial dependencies within this domain. We use the official implementation at https://github.com/microsoft/StemGNN.
- CrossGNN [14] constructs multi-scale time series with varying noise levels through adaptive multi-scale identifiers, subsequently capturing temporal dependencies and variable correlations by cross-scale GNN and cross-variable GNN. We use the official implementation at https://github.com/hqh0728/CrossGNN.
- FourierGNN [34] initially establishes a hypervariate graph and transforms features into the Fourier space. It then stacks Fourier graph operators in the Fourier domain to capture temporal-spatial dependencies. We use the official implementation at https://github.com/aikunyi/FourierGNN.
- **GRU-D** [7] is a model based on gated recurrent units, employs time decay and missing data imputation strategies to address irregularly sampled time series. We use the official implementation at https://github.com/zhiyongc/GRU-D.
- **SeFT** [12] transforms time series into a set of embeddings and then uses a set of functions to model them, offering excellent parallelism and efficient memory usage. We use the open source implementation at https://github.com/mims-harvard/Raindrop.
- RainDrop [41] represents each sample as an independent sensor graph, capturing temporal dependencies between sensors through innovative message-passing operators. It infers the underlying sensor graph structure and uses it alongside proximate observations to forecast unaligned readings. We use the official implementation at https://github.com/mims-harvard/Raindrop.
- Warpformer [37] is a Transformer-based model, adopts a tailored input representation that explicitly encapsulates both intra-series inconsistency and inter-series asynchrony. It produces multi-scale representations that balance coarse-grained and fine-grained signals for subsequent tasks. We use the official implementation at https://github.com/imJiawen/Warpformer.

- mTAND [25] is an IMTS imputation model that can be easily applied to forecasting tasks by only replacing the queries for imputation with forecasting. It learns embeddings for numerical values corresponding to continuous time steps and generates fixed-length representations for variable-length sequential data using an attention mechanism. We use the official implementation at https://github.com/reml-lab/mTAN.
- Latent-ODE [22] enables recurrent neural networks to have continuous-time hidden state dynamics specified by neural ODEs. We use the official implementation at https://github.com/YuliaRubanova/latent\_ode.
- CRU [23] handles irregular intervals between observations by evolving the hidden state based on a linear stochastic differential equation and the continuous-discrete Kalman filter. We use the official implementation at https://github.com/boschresearch/Continuous-Recurrent-Units.
- **Neural Flow** [2] models the solution curves of ODEs through neural networks to mitigate the expensive solvers in neural ODEs. We use the official implementation at https://github.com/mbilos/neural-flows-experiments.
- **GraFITi** [33] converts the time series to a sparsity structure graph which is a sparse bipartite graph, and then reformulates the forecasting problem as the edge weight prediction task in the graph. It uses the power of GNN to learn the graph and predict the target edge weights. We use the official implementation at https://github.com/yalavarthivk/GraFITi.
- **T-PatchGNN** [39] proposed a transformable patch method for converting univariate irregular time series into temporally aligned patches of variable lengths. These patches are then fed into the Transformer module and the temporal adaptive GNN to capture temporal dependencies and dynamic variable correlations. We use the official implementation at https://github.com/usail-hkust/t-PatchGNN.

### **B.3** Implementation

We train the model using the Adam [16] optimizer with an initial learning rate of 0.001. The batch size is fixed at 32, and the maximum number of epochs is set to 1000. Early stopping is applied if the validation loss does not decrease within 40 epochs to prevent overfitting. We use CosineAnnealingLR to adjust the specific learning rate for each epoch, with a fixed adjustment period of 40 epochs.

Optimal hyperparameters for AiT are determined via grid search. The hidden dimension of each module is fixed at 64 (selected from 16, 32, 64, and 128). The numbers of attention heads and Transformer blocks in the Spatial Encoder are set to 4 (selected from 1, 2, 4, and 8) and 3 (selected from 1, 2, 3, and 4), respectively. Appendix C.1 provides a detailed hyperparameter sensitivity analysis. It is important to note that, in contrast to T-PatchGNN [39], which optimizes parameters individually for each dataset, we employ a consistent hyperparameter configuration across all datasets to evaluate generalizability and mitigate deployment complexity. With dataset-specific tuning, the performance of AiT can be further enhanced.

To facilitate open science and community collaboration, we will make all data, source code, and pre-trained weight checkpoints publicly accessible following the release. These resources will offer substantial support for subsequent research. All experiments are implemented using Python 3.10.13 and PyTorch 2.1.2, and executed on an Ubuntu server equipped with an AMD Ryzen 9 7950X 16-core processor and a single NVIDIA GeForce RTX 4090 GPU. To mitigate randomness, we perform each experiment using five different random seeds and present the mean and standard deviation of results.

## **B.4** Ablation Study

To validate the effectiveness and reasonableness of each component, we evaluate the performance of AiT and its variants across all datasets. The detailed descriptions of these variants are as follows:

• rp TTCN: We substitute ALinear in the Temporal Encoder with a Transformable Time-aware Convolution Network (TTCN) [40], which is widely employed in previous IMTS forecasting frontier algorithms [39]. TTCN adaptively derives the time-aware convolution filter corresponding to the length of the input series through a meta-filter. It offers flexibility to adapt to variable-length series through transformable filters and customs parameterization for varying time intervals in IMTS.

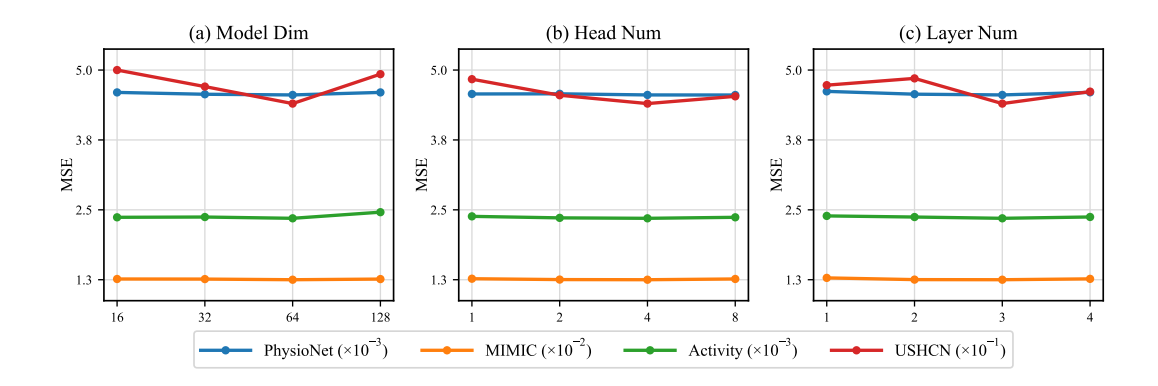


Figure 4: The prediction error of AiT with various hyperparameter configurations for irregular multivariate time series forecasting. A lower value denotes superior prediction accuracy.

- rp TempTF: We substitute ALinear in the Temporal Encoder with the Transformer+Pool architecture, which is widely employed in previous IMTS forecasting frontier algorithms [38]. This architecture initially constructs a unified representation for observations with time point, variable, and numerical embedding. Subsequently, the Transformer captures the dependencies among different observations through a self-attention mechanism. Ultimately, a representation vector of fixed dimension is produced by applying an average pooling to the sequence of hidden vectors derived from all observations.
- rm SpatTF: We remove the Spatial Encoder. The combined embedding  $\mathbf{h}^n$  resulting from the dynamic variable representation  $\mathbf{h}^n_{\text{dyna}}$  and static variable representation  $\mathbf{h}^n_{\text{stat}}$  is sent directly to the Predictor to derive query series.
- rm StatVE: We remove the static variable representation  $\mathbf{h}_{\text{stat}}^n$  and the subsequent Projection employed to uphold dimension consistency. Equation 5 simplifies to retaining solely the dynamic variable representation  $\mathbf{h}^n = \mathbf{h}_{\text{dyna}}^n$ .
- rp TsMLP: We replace ALinear in the Predictor with an MLP architecture, which is widely employed in previous IMTS forecasting frontier algorithms [39]. This MLP structure comprises two layers of linear transformations and an activation function of ReLU. It takes as input the forecasting query embedding  $\phi\left(q_{j}^{n}\right)$  and the comprehensive representation  $\mathbf{h}^{n}$  of the relevant variables modeled by the Temporal and Spatial Encoders, subsequently yielding the corresponding prediction values  $\hat{x}_{j}^{n}$ . This operation can be articulated as follows:  $\hat{x}_{j}^{n} = \text{MLP}\left(\left[\mathbf{h}^{n} \| \phi\left(q_{j}^{n}\right)\right]\right)$ , where  $\phi(\cdot)$  denotes the mapping function that transforms  $q_{j}^{n}$  into the hidden space.

#### C Full Experimental Result

#### C.1 Hyperparameter Analysis

To evaluate the sensitivity of the AiT model for various hyperparameter selections, we design and conduct a series of experiments to investigate the prediction performance of AiT across multiple hyperparameter configurations. Essential hyperparameters include the dimension of the hidden layer vectors, the number of heads in the multi-head self-attention mechanism within each Transformer block, and the number of stacks of Transformer blocks in the Spatial Encoder. Figure 4 summarizes the experimental results across four real-world datasets, illustrating the variation in model performance under different hyperparameter settings.

The dimension of the hidden vectors directly influences the learning capacity and expressive potential of AiT. Smaller hidden vector dimension, while reducing computational resource requirements, may hinder the model from capturing intricate data features, potentially leading to information loss and a decline in prediction accuracy. Conversely, larger hidden vector dimension can enhance the capacity to identify complex patterns, thereby improving expressive power and generalization ability. However, this also proportionately increases computational overhead and may induce overfitting, particularly

Table 5: The prediction errors of AiT and baselines for irregular multivariate time series forecasting across different observation and forecasting horizons. The results of iTransformer and GraFITi are reproduced from their official implementations and other results are taken from T-PatchGNN. A lower value denotes superior prediction accuracy. The optimal and suboptimal results are highlighted in bold and underlined, respectively.

Method	3 h ===	⇒ 45 h	12 h =	⇒ 36 h	36 h =	⇒ 12 h	45 h =	⇒ 3 h
	$MSE \times 10^{-3}$	${\rm MAE}{\times}10^{-2}$	$MSE \times 10^{-3}$	${\rm MAE}{\times}10^{-2}$	$MSE \times 10^{-3}$	${\rm MA}{\times}10^{-2}$	$MSE \times 10^{-3}$	$MAE \times 10^{-2}$
iTransformer	$60.6 \pm 0.65$	$20.2 \pm 0.60$	$59.3 \pm 0.71$	$18.6 \pm 0.55$	$49.7 \pm 0.55$	$16.7 \pm 0.48$	$47.7 \pm 0.51$	$16.2 \pm 0.41$
DLinear	$51.8 \pm 0.01$	$17.1 \pm 0.05$	$43.6 \pm 0.12$	$15.7 \pm 0.05$	$41.6 \pm 0.03$	$15.5 \pm 0.04$	$41.2 \pm 0.05$	$15.5 \pm 0.03$
TimesNet	$57.3 \pm 0.09$	$10.7 \pm 0.07$	$25.0 \pm 0.11$	$7.62 \pm 0.04$	$13.6 \pm 0.12$	$5.50 \pm 0.03$	$13.9 \pm 0.09$	$5.65 \pm 0.03$
PatchTST	$42.2 \pm 0.28$	$13.7 \pm 0.16$	$18.6 \pm 0.27$	$7.80 \pm 0.17$	$9.85 \pm 0.23$	$5.11 \pm 0.13$	$8.53 \pm 0.17$	$4.64 \pm 0.12$
Crossformer	$9.48 \pm 0.11$	$5.86 \pm 0.16$	$8.57 \pm 0.16$	$5.70 \pm 0.13$	$5.70 \pm 0.14$	$4.47\pm0.12$	$5.33 \pm 0.06$	$4.44\pm0.09$
Graph Wavenet	$9.43 \pm 0.29$	$5.86 \pm 0.13$	$7.23 \pm 0.25$	$4.82 \pm 0.12$	$4.71 \pm 0.22$	$3.90 \pm 0.10$	$4.10 \pm 0.23$	$3.73 \pm 0.10$
MTGNN	$9.83 \pm 0.27$	$5.95 \pm 0.11$	$7.48 \pm 0.21$	$5.01\pm0.08$	$5.08 \pm 0.17$	$3.99 \pm 0.08$	$5.22 \pm 0.13$	$4.19\pm0.06$
StemGNN	$8.70 \pm 0.27$	$5.37 \pm 0.21$	$7.46 \pm 0.25$	$4.84 \pm 0.21$	$6.65 \pm 0.25$	$4.69 \pm 0.19$	$5.47 \pm 0.21$	$4.56\pm0.16$
CrossGNN	$10.4 \pm 0.34$	$6.56\pm0.17$	$7.97 \pm 0.35$	$5.37 \pm 0.14$	$6.87 \pm 0.29$	$4.73\pm0.12$	$4.80 \pm 0.29$	$4.24\pm0.10$
FourierGNN	$9.59 \pm 0.36$	$5.61 \pm 0.14$	$7.95 \pm 0.39$	$4.99 \pm 0.14$	$6.35 \pm 0.33$	$4.61\pm0.11$	$5.37 \pm 0.29$	$4.34 \pm 0.10$
GRU-D	$8.18 \pm 0.13$	$4.99 \pm 0.09$	$6.89 \pm 0.08$	$4.55 \pm 0.06$	$4.42 \pm 0.08$	$3.66 \pm 0.05$	$4.44 \pm 0.07$	$3.79 \pm 0.05$
SeFT	$9.78 \pm 0.18$	$5.55\pm0.12$	$9.30 \pm 0.19$	$5.41 \pm 0.11$	$9.15 \pm 0.15$	$5.15\pm0.08$	$8.76 \pm 0.16$	$5.57 \pm 0.07$
RainDrop	$10.5 \pm 0.04$	$5.72 \pm 0.11$	$9.89 \pm 0.11$	$5.62 \pm 0.07$	$9.70 \pm 0.07$	$5.40 \pm 0.06$	$9.28 \pm 0.08$	$5.62 \pm 0.06$
Warpformer	$8.48 \pm 0.43$	$5.13\pm0.16$	$7.57 \pm 0.38$	$4.83 \pm 0.14$	$5.60 \pm 0.33$	$4.09 \pm 0.12$	$6.44 \pm 0.29$	$4.67 \pm 0.10$
mTAND	$8.45 \pm 0.31$	$5.23\pm0.21$	$7.11 \pm 0.29$	$4.67 \pm 0.21$	$5.71 \pm 0.20$	$4.17 \pm 0.16$	$5.44 \pm 0.18$	$4.33 \pm 0.14$
Latent-ODE	$8.25 \pm 0.69$	$5.04 \pm 0.33$	$7.20 \pm 0.63$	$4.69 \pm 0.28$	$6.70 \pm 0.53$	$4.36 \pm 0.25$	$7.10 \pm 0.46$	$5.33 \pm 0.21$
CRU	$9.20 \pm 0.34$	$5.38 \pm 0.11$	$9.20 \pm 0.33$	$5.31 \pm 0.10$	$9.50 \pm 0.23$	$5.41 \pm 0.10$	$11.6 \pm 0.20$	$6.98 \pm 0.08$
Neural Flow	$8.30 \pm 0.10$	$4.99 \pm 0.06$	$8.50 \pm 0.07$	$5.27 \pm 0.05$	$7.70 \pm 0.06$	$4.68 \pm 0.05$	$7.40 \pm 0.04$	$5.10 \pm 0.03$
GraFITi	$8.21 \pm 0.32$	$5.14 \pm 0.22$	$6.95 \pm 0.26$	$4.45\pm0.21$	$4.97 \pm 0.25$	$3.99 \pm 0.18$	$4.78 \pm 0.22$	$3.95\pm0.16$
T-PatchGNN	$\underline{8.01\pm0.08}$	$4.87 \pm 0.03$	$6.48 \pm 0.09$	$\underline{4.19 \pm 0.04}$	$4.14 \pm 0.06$	$3.31 \pm 0.04$	$3.69 \pm 0.04$	$\underline{3.25\pm0.03}$
Ours	$\textbf{7.74} \pm \textbf{0.07}$	$\textbf{4.72} \pm \textbf{0.03}$	$5.95 \pm 0.06$	$\textbf{3.95} \pm \textbf{0.03}$	$3.67 \pm 0.05$	$\textbf{3.03} \pm \textbf{0.02}$	$3.49 \pm 0.03$	$\textbf{2.91} \pm \textbf{0.03}$
Impr.	Impr. 3.31 %		7.01 %		9.97 %		8.09 %	

when the training sample size is limited in IMTS. As illustrated in Figure 4(a), at a hidden vector dimension of 128, significant overfitting emerges on two datasets, Activity, which contains the fewest samples, and USHCN, which comprises the least number of variables. In contrast, PhysioNet and MIMIC exhibit greater insensitivity to variations in the dimension of the hidden vectors.

The number of heads in the multi-head self-attention mechanism constitutes a pivotal factor influencing the efficiency of AiT in extracting complex dependencies from the input series. Increasing the number of heads enables the model to learn information from multiple subspaces concurrently, theoretically enhancing its capability to process complex patterns. However, this is accompanied by increased computational costs and memory usage. Conversely, reducing the number of heads decreases model complexity, accelerates the training process, and minimizes required computational resources. Yet, it may impair the ability to capture different features, particularly in tasks necessitating an understanding of higher-order interactions. As illustrated in Figure 4(b), the PhysioNet, MIMIC and Activity datasets exhibit greater stability to variations in the number of heads. In contrast, the performance on USHCN first increases and then decreases as the number of heads increases.

The number of layers of stacked Transformer blocks within the Spatial Encoder influences the capacity to represent high-level semantic features. Deeper network architectures are advantageous for uncovering intricate associations and global patterns in the data. However, they also elevate the risk of overfitting, extend training durations, and increase computational costs. Conversely, a shallower architecture constrains the capacity to manage highly abstract features yet effectively mitigates overfitting, accelerates model training, and conserves hardware resources. As illustrated in Figure 4(c), PhysioNet, MIMIC and Activity exhibit enhanced robustness across varying numbers of Transformer layers in Spatial Encoder. In contrast, the prediction accuracy on USHCN is more sensitive to the number of layers, exhibiting more pronounced fluctuations.

#### C.2 Varying Horizon

Theoretically, the prediction accuracy of a model should progressively enhance as the volume of available historical data increases. Nevertheless, previous studies [36] have demonstrated that an extended historical horizon does not always improve the performance. This counterintuitive phenomenon may stem from the inability of the model to leverage the temporal information within the historical horizon effectively [19]. To assess the effectiveness of AiT and baselines in capturing

Table 6: The prediction errors of ALinear and backbones for regular multivariate time series forecasting. A lower value denotes superior prediction accuracy. The optimal results are highlighted in bold.

Method		NLinear		rp ALinear		iTransformer		rp ALinear		Impr.
		$MSE \times 10^{-1}$	${\rm MAE}{\times}10^{-1}$	$MSE \times 10^{-1}$	${\rm MAE}{\times}10^{-1}$	$MSE \times 10^{-1}$	${\rm MAE}{\times}10^{-1}$	${\rm MSE}{\times}10^{-1}$	$MAE \times 10^{-1}$	
Electricity	96 192 336 720	$1.99 \pm 0.12$ $2.14 \pm 0.05$	$\begin{array}{c} \textbf{2.77} \pm \textbf{0.08} \\ \textbf{2.81} \pm \textbf{0.04} \\ \textbf{2.96} \pm \textbf{0.07} \\ \textbf{3.28} \pm \textbf{0.04} \end{array}$	$2.04 \pm 0.11$ $2.17 \pm 0.07$	$2.83 \pm 0.07$ $2.97 \pm 0.07$	$1.64 \pm 0.07$ $1.77 \pm 0.06$		$1.67 \pm 0.06$ $1.79 \pm 0.11$	$2.59 \pm 0.02$ $2.73 \pm 0.12$	-0.93 %
Traffic	96 192 336 720	$4.57 \pm 0.07$ $4.62 \pm 0.06$	$3.53 \pm 0.11$	$4.57 \pm 0.12  4.62 \pm 0.03$	$3.46 \pm 0.14$ $3.48 \pm 0.07$	$\begin{array}{c} \textbf{3.22} \pm \textbf{0.07} \\ \textbf{3.28} \pm \textbf{0.09} \end{array}$	$\begin{array}{c} \textbf{2.58} \pm \textbf{0.10} \\ \textbf{2.75} \pm \textbf{0.12} \\ \textbf{2.74} \pm \textbf{0.04} \\ \textbf{2.93} \pm \textbf{0.06} \end{array}$	$\begin{array}{c} 3.27 \pm 0.08 \\ 3.30 \pm 0.07 \end{array}$	$2.78 \pm 0.08$ $2.78 \pm 0.07$	0.49 %
In	Impr.   -0.18 %			0.05 %				-0.08 %		

temporal information within the historical horizon, we evaluate model performance across various historical horizons and forecasting horizons. The performance of each algorithm is evaluated under longer-horizon (forecast next 36/45 hours using historical 12/3 hours) and shorter-horizon (forecast next 12/3 hours using historical 36/45 hours) forecasting on PhysioNet. The results are summarized in Table 5.

The experimental results demonstrate that AiT consistently outperforms all other models across various horizons. Although the performance of most models improves with an extended historical horizon, the algorithms based on ODEs exhibit a decline in performance when using a longer history to forecast shorter horizons. This may be because the too-long sequence and less labeled data degrade the performance of this type of method [39]. Furthermore, when the historical horizon is significantly reduced (e.g., 3 hours), the performance disparity among different models tends to decrease. This may be attributed to the limited available information, making it relatively easier for all models to capture the critical features. Notably, our models demonstrate more substantial improvements when addressing longer historical horizons (e.g., a 9.97% enhancement for 36 hours and a 8.09% enhancement for 45 hours) compared to shorter historical horizons (3.31% enhancement for 3 hours and 7.01% enhancement for 12 hours). This finding suggests that adaptive linear network possess the capability to effectively leverage sparse information from a limited number of observations for capturing temporal dependencies.

#### **C.3** Module Generality

To validate the applicability of ALinear for RMTS forecasting, we specifically design a series of supplementary experiments. These experiments utilize Electricity and Traffic datasets [28], which are extensively used for benchmarking in the RMTS domain and are publicly accessible. We follow the standard segmentation protocol [19], strictly dividing each dataset into training, validation, and testing sets chronologically to ensure no information leakage issues. The segmentation ratio for each dataset is set to 6:2:2. Regarding forecasting settings, we also adhere to established mainstream protocols [36]. Specifically, we set the length of the historical horizon to 96, while the forecasting length varies within {96, 192, 336, 720}. Unless otherwise indicated, the remaining experimental setups align with Section 4.1.

We select two mainstream methods as baselines for comparison: NLinear [36] and iTransformer [19]. NLinear employs a standard linear network with static weights to independently process each variable, and generate the predictions through a weighted summation of historical data. Conversely, iTransformer supplements a Transformer architecture based on NLinear, aiming to capture variable correlations via an attention mechanism [27] to enhance prediction accuracy. It first extracts temporal features from the raw series of each variable independently using a standard linear network. Then, the transformer architecture is utilized to capture correlations between variables. Ultimately, the embedding will be projected into the forecasting series through another standard linear network. In this study, we substitute the traditional linear networks used to model temporal dependencies in both aforementioned methods with ALinear.

Table 6 presents the results of MSE and MAE evaluations for NLinear, iTransformer, and its variants across both datasets. The experimental findings indicate that the overall prediction performance of the model experiences minimal variation following the replacement of the ALinear. Although minor

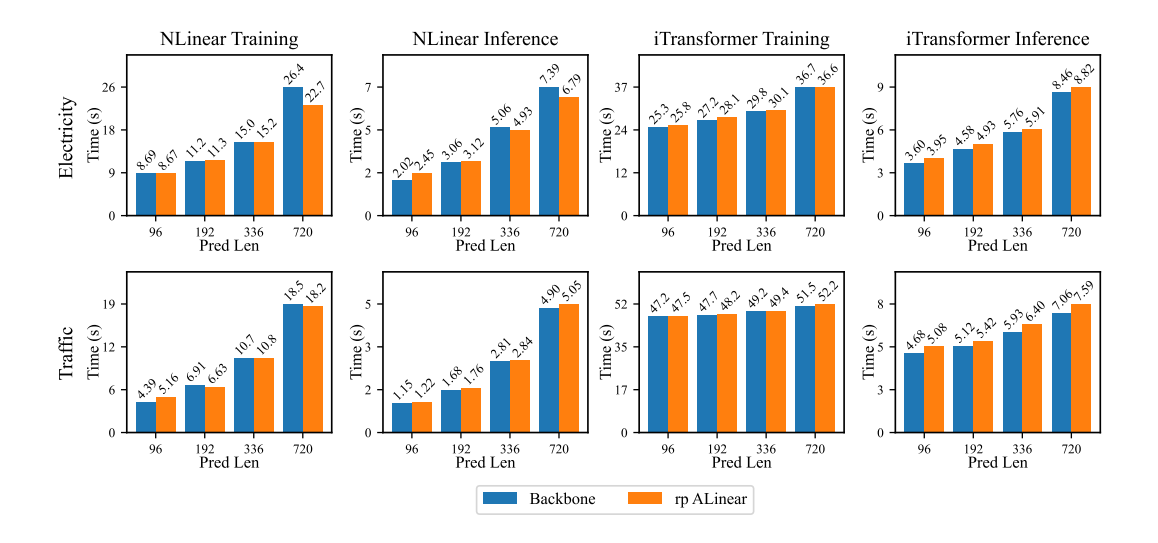


Figure 5: The average training time per epoch and total inference time of ALinear and backbones for regular multivariate time series forecasting. A lower value denotes greater efficiency.

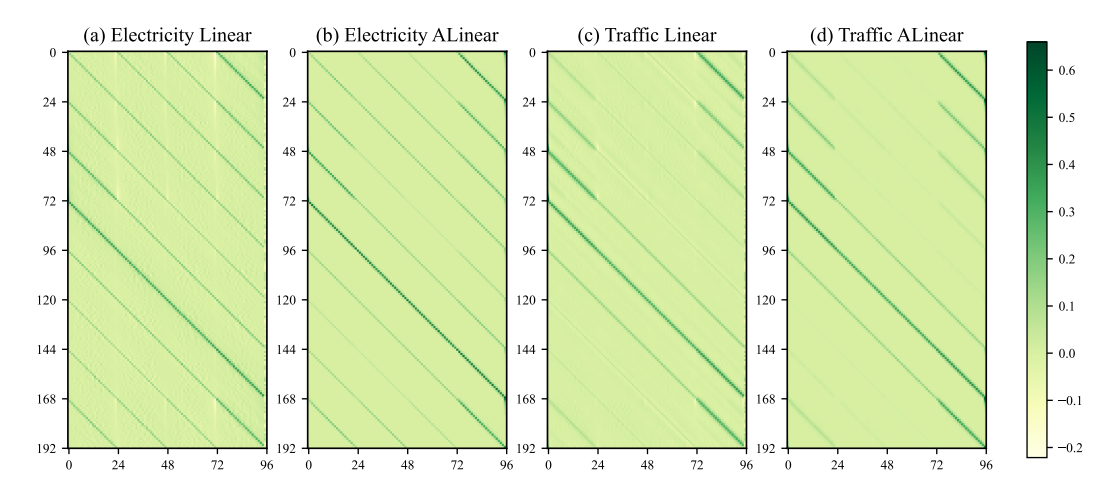


Figure 6: The forecasting weights of ALinear and backbones for regular multivariate time series forecasting. A deeper color denotes higher weight.

fluctuations are observed, these changes remain within the 1% threshold and do not represent a statistically significant difference. Furthermore, we explore the differences in computational efficiency between adaptive linear network and standard linear network. As illustrated in Figure 5, the time consumed by these two architectures is approximately equivalent across various scenarios. However, it is noteworthy that when faced with a longer horizon, ALinear exhibits enhanced computational efficiency due to the utilization of more efficient dot-product attention derived from two low-dimensional matrices, in contrast to the original high-dimensional matrices [13].

Additionally, Figure 6 visually contrasts the high-dimensional matrix in the standard linear networks with the dot-product attention score matrix of the two low-dimensional matrices within ALinear. The length of the historical horizon is set to 96, and the length of the forecasting horizon is set to 192. In both instances, the final forecasting series is attained by weighting and summing the historical data according to the corresponding matrices [26]. A graphical comparison shows that the two matrices are nearly identical, confirming the capacity of ALinear to effectively address data modeling and forecasting tasks for regular and irregular time series.

## **D** Broader Impact

In this work, our core contribution lies not in proposing an elaborate model, but in demonstrating the practical feasibility of a simple, intuitively inspired design. Compared to previous baselines, which are often elaborate and computationally expensive, ALinear achieves excellent prediction accuracy and significantly improves computational efficiency, showing its superiority in real-world applications. It will positively influence numerous domains such as finance, transportation, energy, healthcare, climate, etc. Moreover, our work helps bridge the gap between RMTS and IMTS, laying the groundwork for future collaboration and dialogue between the two fields. We hope AiT serves as a simple yet powerful new benchmark for IMTS, inspiring fresh perspectives and further advancements in the area. Upon acceptance of the paper, we will make the complete source code and corresponding checkpoints available to facilitate future research. This paper focuses solely on algorithmic design. All codes and datasets are used strictly with their respective licenses (see Appendix B.1 and B.2). There are no foreseeable ethical risks or negative societal impacts associated with this work.

# **E** Limitation

This study proposes the AiT method and validates its performance on four real-world datasets. However, there remain several key limitations that warrant further investigation and improvement. First, the current experiments primarily focus on the healthcare and climate domains, leaving the model's generalizability to other scenarios, such as finance and transportation, largely untested. These domains often involve high-frequency sampling, extreme noise, or more complex dynamic patterns, which are not fully captured in the existing experiments. This limits the applicability and versatility of the proposed method. Second, the performance of AiT is highly dependent on the stationarity of the data distribution. When there is a significant temporal shift between the training and testing sets, the model may struggle to accurately capture dependencies within the time series, thereby compromising its ability to model complex relationships among variables. In summary, future work should aim to refine the model design and explore a broader range of application scenarios to enhance the generalizability and robustness of AiT.